of 150° and 180°. This is, in fact, consistent with Teo's calculations showing that the scattering phases are quite similar between the scattering angles of 0° and 30° (bridging angles of 180° and 150°), despite the enormous variation of scattering amplitudes. The insensitivity of phase shifts as a function of scattering angles thus allows us to transfer the parameterized phase shifts for distance determination.

### Conclusion

In this paper, we have examined the X-ray absorption spectra of a series of oxygen-bridged iron complexes and demonstrated the effect of the intervening oxygen atom on the analysis of outer-shell iron waves. The results indicated that for compounds of Fe–O–Fe bridging angle ca. 100°, the three scattering pathways are resolvable and can be analyzed independently to find the Fe–Fe distance. When the bridging angle increases, the multiple-scattering pathways become dominant. The multiple-scattering pathway III is signified by an enhancement in amplitude which is directly related to the bridging angle of the system. The largest enhancement is found in the linear Fe–O–Fe system, of which the amplitude of the scattered iron wave is magnified by a factor of 4. The phase is also found to be shifted by approximately $\pi$ in the constant part and about −0.1 Å in the linear part as the photoelectron propagates through the potential of the oxygen atom with a scattering angle of 103°. The variation of the phase as a function of scattering angle in the range of 0° and 30° is found to be small, not significant in the analysis.

The analysis of the series of compounds has shown that for an isolated backscattering peak, it is possible to estimate the bridging angle to ±8° and calculate the metal–metal distance to within ±0.05 Å. This method has been applied to examine a dimeric iron system in hemerythrin and calculates an Fe–O–Fe angle of 165° and an iron–iron distance of 3.38 Å. The work also illustrates that care must be exercised in interpreting EXAFS of neighboring atoms beyond the first coordination shell.

**Acknowledgment.** We thank Dr. H. J. Schugar, Dr. A. W. Addison, Dr. K. S. Murray, Dr. J. A. Bertrand, and Dr. A. T. McPhail for donation of compounds for this study. We also thank Dr. Robert A. Scott, Dr. Janet L. Smith, Jim Hahn, and Steve Conradson for helpful discussions. This work was supported in part by the National Science Foundation through Grant PCM-79-04915. Synchrotron radiation time for the EXAFS work was provided by the Stanford Synchrotron Radiation Laboratory, supported by the National Science Foundation (DMR 77-27489) and the National Institutes of Health (RR-01209).

**Registry No.** I, 58982-68-6; II, 58982-69-7; III, 49788-37-6; IV, 55134-47-9; V, 56968-10-6; VI, 19633-03-5; VII, 51331-59-0; VIII, 20559-32-4; IX, 18024-73-2; X, 19555-43-2; XI, 67477-28-5; XII, 84237-93-4.

# Molybdenum Chalcogenides: Clusters, Chains, and Extended Solids. The Approach to Bonding in Three Dimensions

**Timothy Hughbanks and Roald Hoffmann***

*Contribution from the Department of Chemistry and Materials Science Center, Cornell University, Ithaca, New York 14853.* *Received July 29, 1982*

**Abstract:** A combined molecular orbital and crystal orbital analysis of systems containing $Mo_{3n}X_{3n+2}$ ($n$ = 2, 3, 4, ∞; X = S, Se, Te) units is presented. The modes of packing $Mo_6X_8$, $Mo_9X_{11}$, and $Mo_{12}X_{14}$ clusters into crystals are explained in terms of the cluster frontier orbitals. Intercluster Mo–X bonds are seen to result from an interaction between chalcogen donor orbitals and the cluster LUMO's that are localized on Mo atoms residing in the "square faces" of the clusters. Closed-shell electron counts for the clusters are elucidated. The relationship between the cluster frontier orbitals and surface states is discussed. Finally, relationships between the band structure of $(Mo_3X_3^-)_\infty$ chains and the finite cluster molecular orbitals are explained.

### Structural Overview

For over a decade, compounds known as the "Chevrel phases"[1] have excited solid-state chemists and physicists. The prime reason for sustained interest in these compounds has undoubtedly lain in their conducting properties; these ternary molybdenum chalcogenide materials include both high-temperature and very high-field superconductors.[2] Most of these materials can be described by the formula $MMo_6X_8$, where M = Pb, Sn, Ba, Au, Cu, Li, etc. and X is usually S, Se, or Te (though compounds containing halogens have been prepared). Compounds in which some Mo atoms are replaced by Re, Ru, and Rh have also been made.[3,4]

The fundamental structural unit to be found in the Chevrel phases is the cluster $Mo_6X_8$ displayed in three different and geometrically pleasing ways in **1**. In **1a** an octahedron of molybdenums (Mo–Mo ≅ 2.7 Å) is encased in a cube of chalcogens (Mo–S ≅ 2.45 Å or Mo–Se ≅ 2.6 Å). **1b** exhibits the same cluster as consisting of an octahedron with its triangular faces capped by chalcogenides; this view emphasizes the connectivity within the cluster. In **1c** the cluster has been reoriented so that a 3-fold

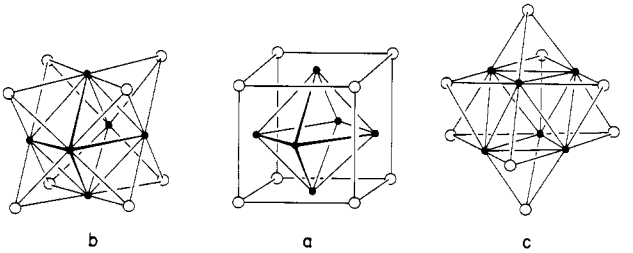


1

(1) Chevrel, R.; Sergent, M.; Prigent, J. *J. Solid State Chem.* **1971**, *3*, 515–519.
(2) For reviews, see: (a) Fisher, Ø. *Appl. Phys.* **1978**, *16*, 1–28. (b) Chevrel, R. In "Superconductor Materials Science: Metallurgy, Fabrication and Applications"; Foner, S., Schwartz, B. B., Eds.; Plenum Press: New York, 1981; Chapter 10.
(3) Perrin, A.; Sergent, M.; Fisher, Ø. *Mater. Res. Bull.* **1978**, *13*, 259.
(4) Perrin, A.; Chevrel, R.; Sergent, M.; Fischer, Ø. *J. Solid State Chem.* **1980**, *33*, 43–47.

0002-7863/83/1505-1150$01.50/0 © 1983 American Chemical Society

axis is vertical. One advantage of this is that it allows a mental decomposition of the cluster into fragments as shown in **2**. The

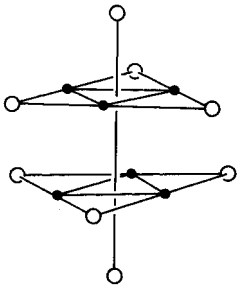

**2**

$Mo_6X_8$ unit is built from two $Mo_3X_3$ planar fragments, staggered and stacked one upon the other, then capped top and bottom by chalcogenides. After all the bonds thus formed are drawn, the view in **1c** is obtained; we will utilize this fragmentation mode in discussing larger clusters below.

Particularly interesting from a structural point of view is the manner in which the $Mo_6X_8$ clusters "pack" in crystals. For compounds such as $PbMo_6S_8$ (well-known as a high-temperature, high-field superconductor, $T_c \cong 14$ K),[5] we can build up the crystal structure in the following way. First, construct a simple cubic array of Pb atoms with a lattice constant of 6.54 Å. Second, place the clusters within the Pb atom cubes thus formed so as to preserve the cubic symmetry of the lattice as in **3**. Finally, rotate each

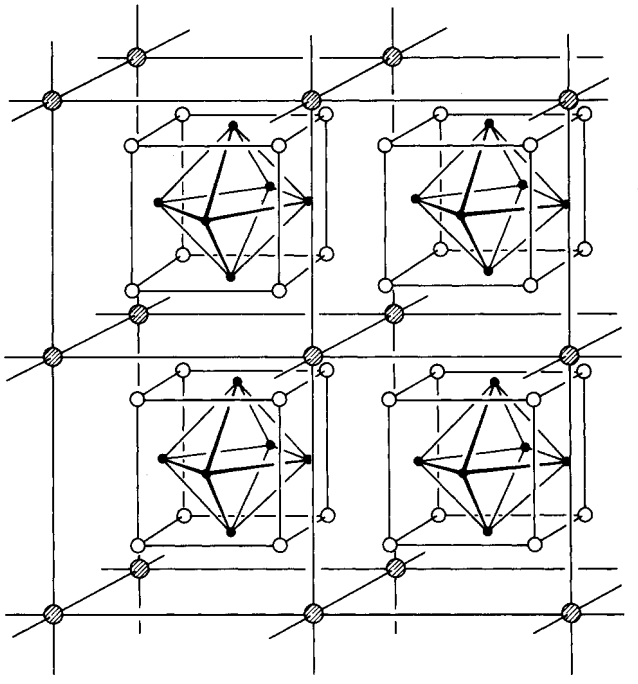

**3** ◎ Pb ○ S • Mo

of the clusters by ~26° about the 3-fold body axes of the Pb cubes (retaining the one cluster per unit cell translational symmetry). This final step is shown in **4**—it should be noted that this deformation breaks the heretofore cubic symmetry of the crystal and a rhombohedral system results. However, the rhombohedral angle is typically about 89°, making this otherwise artificial construction quite accurate in describing the actual atomic positions.

Thus, we have octahedra within cubes, rigidly rotating within other cubes. This description raises a question: why do the clusters

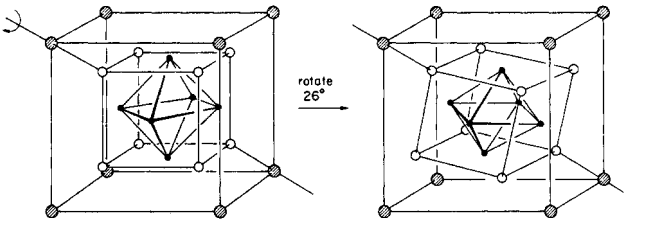


**4**

rotate? This problem was addressed theoretically by Burdett and Lin,[6] who found that intercluster chalcogen–chalcogen repulsions cause the "ideal" structure, **3**, to be greatly disfavored when the unit cell dimensions are fixed at values observed in $PbMo_6S_8$. These chalcogen repulsions were found to be minimized very near the observed rotational angle. The role of chalcogen–chalcogen repulsions, among other matters, is discussed at length by Corbett.[6b]

Despite the conceptual ease of describing the structure of the Chevrel phases with the method of construction outlined above, there are serious drawbacks to this approach. Most importantly, the nature of the actual intercluster contacts is obscured. Also left unsaid is the fact that the M atoms (taken to be Pb in **3** and **4**) do not necessarily form a "simple cubic" array as indicated above. In fact, there is considerable variability in positioning and stoichiometry with regard to the M atoms; a large variety of cations may be intercalated, often reversibly, into the $Mo_6X_8$ host.[6c] Despite this, the main features of the intercluster packing remain intact: the nature of this packing is shown in **5**, where no attempt to show the M atoms is made.

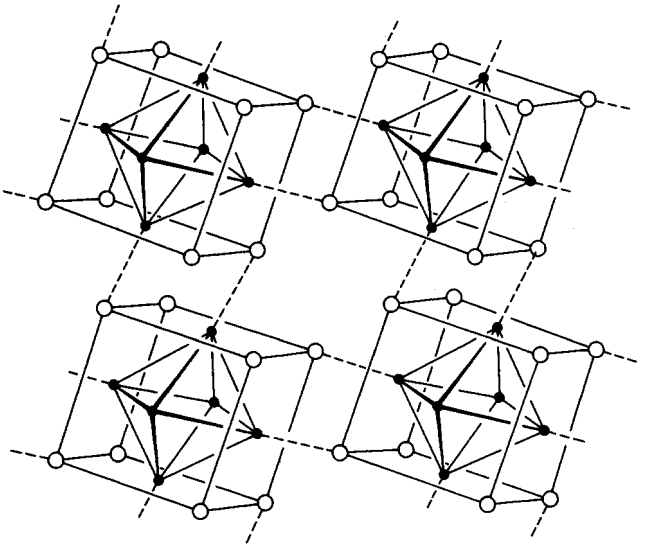

**5** ○ : X = S, Se, Te • : Mo (Re, Ru)

Here we make a point about the intercluster arrangement we feel is crucial: The clusters are packing in such a way as to place chalcogens on neighboring clusters over the Mo atoms in a given cluster. An equivalent statement of this rule might be "Mo atoms that reside in a square-planar site with respect to chalcogen coordination *within* a cluster seek to become square pyramidal by bonding with chalcogens on neighboring clusters". This second statement might seem more general than necessary since *all* Mo atoms in $Mo_6S_8$ are found to be square planar with respect to coordination by intracluster chalcogen atoms; however, in the clusters which we now describe this generalization is important.

Within the last few years, Chevrel, Potel, Sergent, and coworkers have reported the synthesis of compounds containing

(5) Matthias, B. T.; Marezio, M.; Corenzwit, E.; Cooper, A. S.; Barz, H. E. *Science (Washington, D.C.)* **1972**, *175*, 1465–1466.

(6) (a) Burdett, J. K.; Lin, J.-H. *Inorg. Chem.* **1982**, *21*, 5–10. (b) Corbett, J. D. *J. Solid State Chem.* **1982**, *39*, 56–74. (c) Schöllhorn, R. *Angew. Chem.* **1980**, *92*, 1015–1035; *Angew. Chem., Int. Ed. Engl.* **1980**, *19*, 983–1003.

clusters with formulas $Mo_9X_{11}$ (**6**) and $Mo_{12}X_{14}$ (**7**).[2b,7-10] The

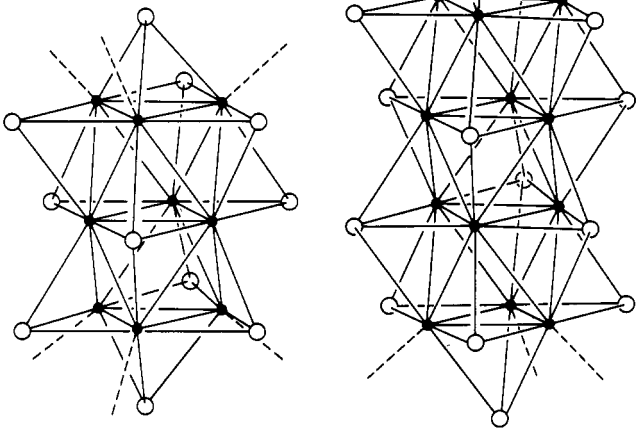

6 7

relationship between these clusters and $Mo_6X_8$ may be seen by thinking in terms of the fragmentation illustrated for $Mo_6X_8$ in **2**. $Mo_9X_{11}$ and $Mo_{12}X_{14}$ can be respectively described as consisting of stacks of three and four staggered $Mo_3X_3$ units which are capped, as before, with chalcogens. The metal–metal and metal–chalcogen distances in these larger clusters are in the same range (2.6 Å ≤ Mo–Mo ≤ 2.8 Å) as in the prototypical $Mo_6X_8$ clusters, but Mo–Mo bonds between $Mo_3X_3$ layers tend to be somewhat longer (~0.1 Å) than within layers. The metal atoms in the top and bottom layers of these clusters are very similar in their environment to the metal atoms in $Mo_6X_8$; indeed, the nearest neighbors of these atoms are identically situated in all the clusters.

In the crystalline compounds in which the $Mo_9X_{11}$ and $Mo_{12}X_{14}$ clusters are found, they do not appear exclusively, at least to date. Instead, these larger clusters have been found to cocrystallize with $Mo_6X_8$ clusters. Thus, $Tl_2Mo_9S_{11}$ contains no $Mo_9S_{11}$ clusters but a 1:1 "mixture" of $Mo_6S_8$ and $Mo_{12}S_{14}$ clusters. $In_{\sim 3}Mo_{15}Se_{19}$ and $Ba_2Mo_{15}Se_{19}$ each contain an equal proportion of $Mo_6Se_8$ and $Mo_9Se_{11}$ units assembled in different ways. We shall not go into the fascinating details of the assemblage of these crystals from the clusters (and counterions) but will recite some salient features. One general rule seems to apply to all the compounds reported: the $Mo_nX_{n+2}$ clusters ($n$ = 2, 3, 4) arrange themselves in such a way as to cap square-planar Mo atoms with chalcogens. Therefore, the similarity between the "terminal" atoms in $Mo_9X_{11}$ and $Mo_{12}X_{14}$ and the metal atoms in $Mo_6X_8$ extends to more than just the intracluster environment; *inter*cluster linkage is also the same. Mo–X intercluster contacts are again comparable to those found within the clusters; the nature of these is illustrated in **8** (cross-hatched atoms are chalcogens on neighboring clusters).

$Mo_6X_8$, $Mo_9X_{11}$, and $Mo_{12}X_{14}$ form a progression which has an infinite chain with stoichiometry $(Mo_3X_3)_\infty$ as its limit. The synthesis of the compounds $M_2Mo_6X_6$ (M = In, Tl, Na, K; X = S, Se, Te) provided the remarkable realization of this limit.[11,12]

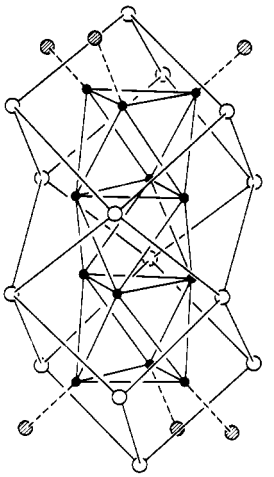

8

The structure of $Tl_2Mo_6Se_6$ is shown in **9**. It is composed of

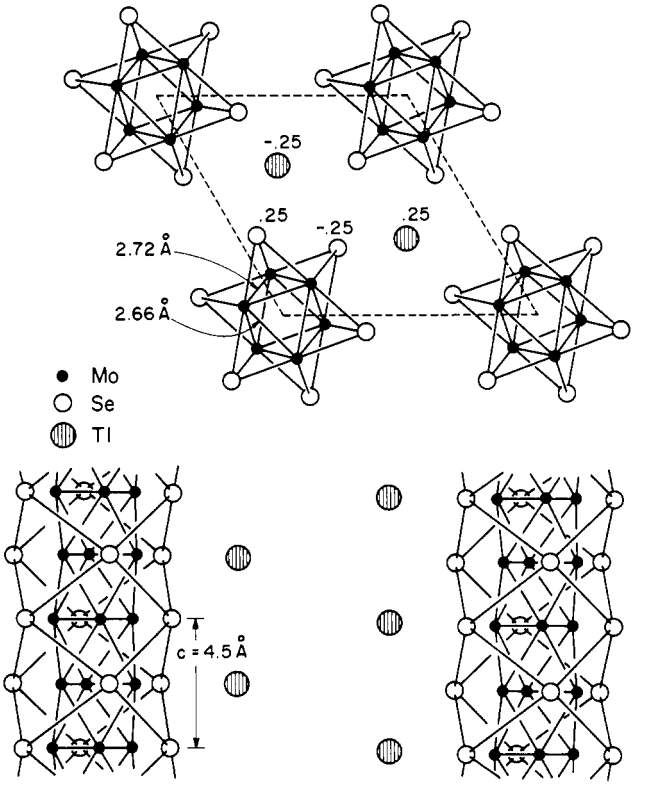


9

staggered stacks of $Mo_3Se_3$ units forming chains which are separated by columns of Tl ions. There are no "terminal" Mo atoms in these chains, and hence there are no close contacts between atoms of different chains. Consequently, the structure is very anisotropic, and a corresponding anisotropy or "one-dimensionality" is expected and observed in the conductivity of these metallic systems.

In the above paragraphs we have given a brief description of the structural characteristics of a beautiful series of compounds in which the evolution from clusters to chains may be clearly seen. In the present work we will give a description of the electronic structure and bonding in these materials which both exploits and explains the various similarities between these obviously closely related compounds. We have seen for example that the intercluster linkages in the cluster compounds are all quite similar structurally. Is there any simple explanation of these structural similarities in terms of the MO's of the clusters? To what extent is the bonding *within* the clusters similar? Clearly these compounds offer a good

(7) Fischer, Ø.; Seeber, B.; Decroux, M.; Chevrel, R.; Potel, M.; Sergent, M. In "Superconductivity in d- and f- Band Metals"; Sohl, H., Maple, M. B., Eds.; Academic Press: New York, 1980; pp 485–499.

(8) Grüttner, A.; Yvon, K.; Chevrel, R.; Potel, M.; Sergent, M.; Seeker, B. *Acta Crystallogr., Sect. B* **1979**, *B35*, 285–292.

(9) Potel, M.; Chevrel, R.; Sergent, M. *Acta Crystallogr., Sect. B* **1980**, *B36*, 1319–1322.

(10) Chevrel, R.; Potel, M.; Sergent, M.; Decroux, M.; Fischer, Ø. *J. Solid State Chem.* **1980**, *34*, 247–251.

(11) Potel, M.; Chevrel, R.; Sergent, M.; Armici, J. C.; Decroux, M.; Fischer, O., *Acta Crystallogr., Sect. B* **1980**, *B36*, 1545–1548.

(12) Potel, M.; Chevrel, R.; Sergent, M. *J. Solid State Chem.* **1980**, *35*, 286–290.

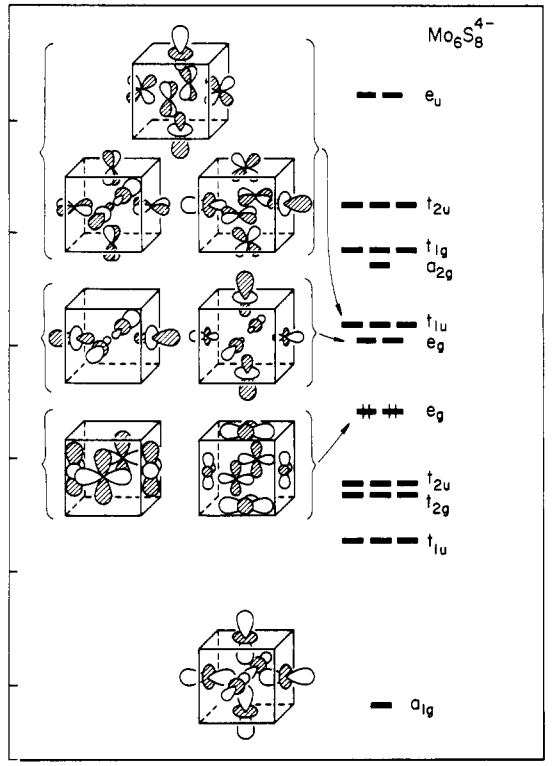


**Figure 1.** Molecular orbitals for $Mo_6S_6^{4-}$. Orbitals explicitly displayed are those with predominantly $z^2$ or $x^2 - y^2$ character.

opportunity to investigate the transition between molecules and extended structures (chains, in this case). For example, how "chain-like" is the $Mo_{12}X_{14}$ cluster?

As we have indicated, the superconducting properties have been the primary impetus for their continued interest. The HOMO of the $Mo_6X_8$ cluster is of crucial importance in the understanding of the superconductivity, as we shall explain below. The $Mo_6X_8$ cluster has been studied by many workers in this regard, but compounds containing $Mo_9X_{11}$ and $Mo_{12}X_{14}$ and their superconducting properties have not been investigated theoretically. Specifically, we will compare the frontier orbitals in all the clusters to give us some clues as to whether the orbitals at the Fermi level in these different systems are similar.

## The $Mo_6X_8$ Cluster

The electronic structure of $Mo_6X_8$ cluster compounds has been the subject of many theoretical studies.[13,14] Nevertheless, we will discuss it here in some detail because of the insight it provides in the study of larger clusters and because the import of the frontier orbitals in understanding the *structural* features of the Chevrel phases has not always been appreciated.

In Figure 1 is the molecular orbital diagram we calculate for the $Mo_6S_8$ cluster, the occupation indicated appropriate for the $Mo_6S_8^{4-}$ species. The levels displayed are all primarily of Mo d character. The sulfur block of levels begins just below the lowest

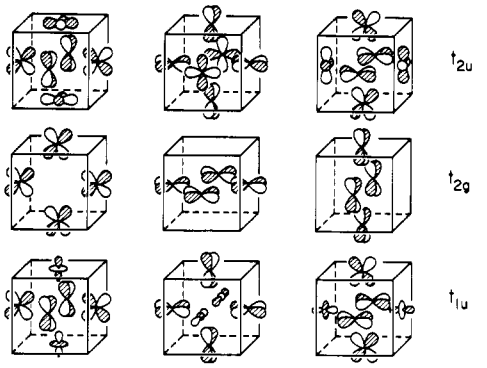


**Figure 2.** Displayed are the Mo–Mo bonding orbitals which are not shown in Figure 1.

$a_{1g}$ level shown. We see that 12 Mo d levels are filled, consistent with an assignment of 24 cluster Mo orbitals based upon an oxidation state of 2– for sulfur.

The symmetry of the $Mo_6S_8$ cluster is so high that the level diagram in Figure 1 can be derived in large part from group theory alone. In discussing these clusters we will adopt a convention in which each metal atom has a local coordinate system such that the "$z$ axes" are normal to the square faces of the cube and the $d_{xy}$ orbitals are directed at the sulfur atoms. With this convention, the representations in the $O_h$ group which are spanned by the metal d orbitals are as follows: $xy$, $a_{2u} + e_u + t_{2g}$; $x^2 - y^2$, $a_{2g} + e_g + t_{2u}$; $z^2$, $a_{1g} + e_g + t_{1u}$; $(xz, yz)$, $t_{1g} + t_{2g} + t_{1u} + t_{2u}$. The $xy$ type orbitals may be safely neglected in considering the Mo–Mo interactions since they are directed at sulfur atoms and hence pushed up (the high-lying $e_u$ orbital in Figure 1 is the lowest of the $xy$ orbitals). The remaining d orbitals are not directed at the sulfur atoms and Mo–Mo interactions are predominantly responsible for the level ordering observed for the metal orbitals in Figure 1. With the $xy$ orbitals eliminated from consideration, the d orbital contribution to the $a_{2g}$, $a_{1g}$, $t_{1g}$, and $t_{2g}$ orbitals are determined solely by symmetry—within the 24-dimensional representation spanned by the $x^2 - y^2$, $z^2$, and $(xz, yz)$ type orbitals on the six metal atoms, each of these four irreducible representations occurs but once. The $e_g$, $t_{1u}$, and $t_{2u}$ representations each occur twice and the metal d contributions to the resultant molecular orbitals will be only slightly more complicated. The $t_{2u}$ orbitals both have significant admixture of $x^2 - y^2$ and $(xz, yz)$. On the other hand, the $e_g$ and $t_{1u}$ MO's can be distinctly characterized as being of either $z^2$ or $x^2 - y^2$ character for the $e_g$ MO's, or, for the $t_{1u}$ MO's, as either $z^2$ or $(xz, yz)$ character. In Figure 2 we show our usual schematic representation of the 12 Mo–Mo bonding orbitals ($t_{1u}$, $t_{2g}$, $t_{2u}$) which are *not* included in Figure 1. Figure 3 displays the LUMO's in orbital plots which contain four Mo atoms from a basal plane of the $Mo_6$ octahedron.

The highest occupied $e_g$ orbitals of the clusters have been previously identified by many workers in the study of the superconductivity of the Chevrel phases. A crucial property of these orbitals is that they are of local $\delta$ symmetry with respect to an axis extending from a metal to the neighbor sulfur atom which caps the square face in which that metal atom resides. Thus we expect from the outset that the HOMO of the cluster will be only weakly perturbed by crystallization since this $\delta$ pseudosymmetry will preclude any strong interaction with neighboring clusters. The situation is very much different as far as the LUMO's are concerned; the $t_{1u}$ and $e_g$ orbitals consist of "$z^2sp_z$" hybrids which are ideally directed for interaction with sulfur atoms on neighboring clusters. To model the effect of neighboring sulfides, we placed six $S^{2-}$ ions over the Mo atoms in the cluster—the resulting $Mo_6S_6^{4-}(S^{2-})_6$ species is isoelectronic and isostructural to the well-known $Mo_6Cl_{14}^{2-}$. The effect of this perturbation on the $Mo_6S_8^{4-}$ cluster is shown in Figure 4.

As expected on the basis of their orbital character, the LUMO's of the cluster are all strongly pushed up by interaction with the sulfides. The lowest $a_{1g}$ orbital, which is also of $z^2$ parentage, is also perturbed significantly. The interaction with the capping

(13) Treatments of molecular systems are found in: (a) Grossman, C. D.; Olsen, D. P.; Duffey, C. H. *J. Chem. Phys.* **1963**, *38*, 73–75. (b) Cotton, F. A.; Haas, T. E. *Inorg. Chem.* **1964**, *3*, 10–17. (c) Kettle, S. F. A. *Theor. Chim. Acta* **1965**, *3*, 211–212. (d) Guggenberger, L. J.; Sleight, A. W. *Inorg. Chem.* **1969**, *8*, 2041–2149. (e) Cotton, F. A.; Stanley, G. G. *Chem. Phys. Lett.* **1978**, *58*, 450–453.

(14) Treatments with emphasis on the applications to the Chevrel phases include: (a) Mattheiss, L. F.; Fong, C. Y. *Phys. Rev. B: Solid State* **1977**, *B15*, 1760–1768. (b) Andersen, O. K.; Klose, W.; Nohl, H. *Ibid.* **1978**, *B17*, 1209–1237. (c) Nohl, H.; Klose, W.; Andersen, O. K. In "Superconductivity in Ternary Compounds"; Fischer, Ø., Maple, M. B., Eds.; 1981; Chapter 6. (d) Bullett, D. W. *Phys. Rev. Lett.* **1977**, *39*, 664–666. (e) Jarlborg, T.; Freeman, A. J. *J. Magn. Magn. Mater.* **1980**, *15–18*, 1579–1580; *Phys. Rev. Lett.* **1980**, *44*, 178–182; additional work by these authors has been submitted for publication. (f) Le Beuze, A.; Makhyoun, M. A.; Lissilour, R.; Chermette, H. *J. Chem. Phys.*, submitted for publication. See also: Le Beuze, A.; Lissilour, R.; Chermette, H.; Potel, M.; Chevrel, R.; Sergent, M. *Solid State Commun.* **1982**, *43*, 19–23.

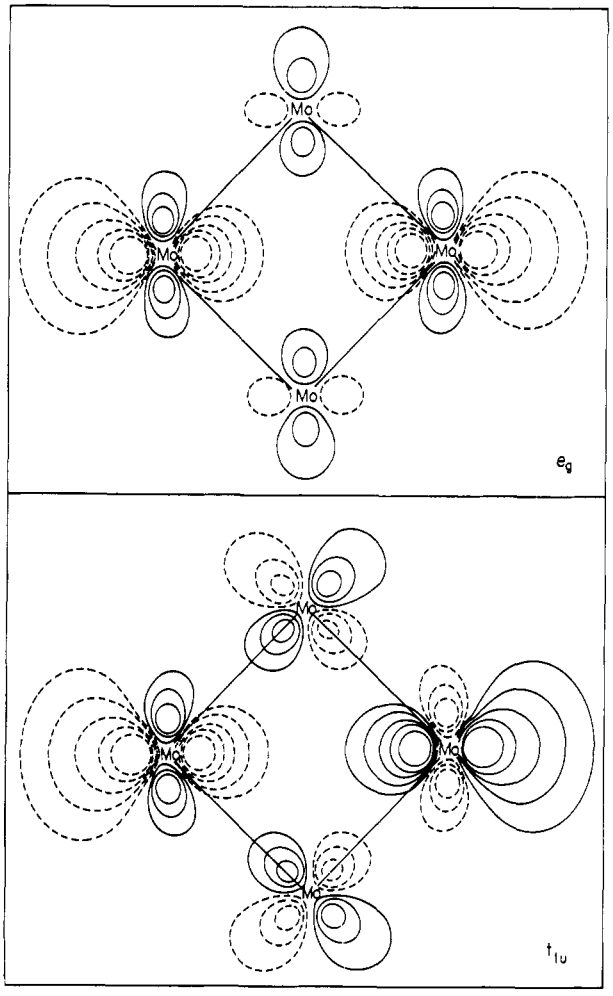


**Figure 3.** Contour plots of single members of the LUMO $e_g(z^2)$ and $t_{1u}(z^2)$ orbitals. The contours of $\psi$ displayed are ±0.20, ±0.15, ±0.10, ±0.06, ±0.03.

sulfides induces sp mixing into the $a_{1g}$ orbital, preventing as large an energy shift as experienced by the LUMO's. The remaining cluster orbitals are perturbed only to a small extent in comparison and this model calculation clearly suggests that the principal structure determining interaction between clusters in the Chevrel phases is this donor–acceptor interaction between sulfides on neighboring clusters and the LUMO $e_g$ and $t_{1u}$ orbitals of a given cluster. Note that the $1e_g$ (HOMO) orbital is virtually unperturbed by the capping sulfides, as expected.

An appreciable HOMO–LUMO gap is opened up by the "removal" of the $2e_g$ and $2t_{1u}$ hybrid orbitals. If we assume that our model accounts for the most important intercluster interactions (which is reasonable in view of the remaining rather long intercluster contacts, ≥3.1 Å), then we expect that compounds with a formal 4–charge on the clusters (or 24 cluster electrons) will be semiconductors. That is, it would be difficult to imagine that the energy bands, which can be thought of as consisting of a broadened version of the cluster orbitals, would be so perturbed as to close the 1.3-eV gap we obtain for the cluster. This suspicion is strongly reinforced by the fact that the "new" LUMO is an orbital of $a_{2g}$ symmetry as shown in **10**. This orbital has "$\delta$"

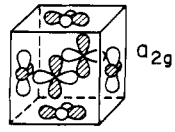


**10**

pseudosymmetry in the same sense as the $1e_g$ HOMO and we

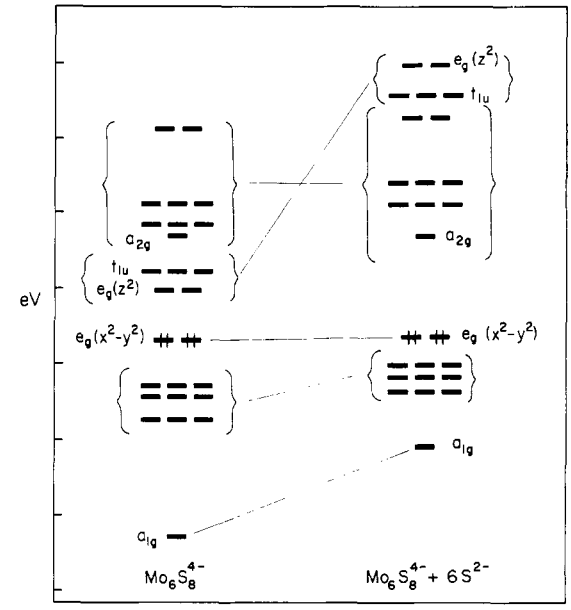


**Figure 4.** Perturbation of $Mo_6S_8^{4-}$ levels by six capping $S^{2-}$ ions. Levels which are weakly perturbed are unlabeled, except for $e_g(x^2 - y^2)$ and the "new" LUMO $a_{2g}$ orbitals.

expect the band formed from this orbital to be quite narrow. As a result, neither the HOMO or LUMO would be expected to give rise to broad enough bands to close the gap seen for the cluster. The 24-electron compounds $Mo_2Re_4S_8$ and $Mo_4Ru_2Se_8$ are semiconducting[3,4]—in satisfying agreement with our expectations based upon the arguments above. In addition, intercalants of the $Mo_6X_8$ systems consistently saturate such that the formal cluster electron count is less than or equal to 24,[6c] indicative of the presence of a gap above this level.

**Band Structure Calculations for the $Mo_6S_8$ System.** Our examination of the $Mo_6S_8$ cluster orbitals has provided a model for understanding the structure of the Chevrel phase compounds. In this section we will see to what extent we can extract support for this model from band structure calculations. Because band structure methods are not as familiar to chemists as their molecular orbital counterparts, we will also explain some of the details of the calculations.

In performing LCAO calculations for crystalline solids (i.e., tight binding calculations), one begins with a symmetry-adapted basis set of orbitals ($\phi_\mu(\vec{k})$), which are Bloch sums of AO's of the unit cells ($\chi_\mu$):

$$\phi_\mu(\vec{k}) = \frac{1}{N^{1/2}}\sum_{\vec{R}} e^{i\vec{k}\cdot\vec{R}}\chi_\mu(\vec{r} - \vec{R}) \qquad (1)$$

The sum over $\vec{R}$ is a summation over the $N$ unit cells of the crystal; the function $\chi_\mu(\vec{r} - \vec{R})$ is the $\mu^{th}$AO of a unit cell at the lattice site specified by $\vec{R}$. The factor $e^{i\vec{k}\cdot\vec{R}}$ specifies the phase change in the orbitals $\{\phi_\mu(\vec{k})\}$ upon moving from a given reference unit cell (at the origin) to a unit cell at the site specified by $\vec{R}$. The set of orbitals ($\phi_\mu(\vec{k})$) are symmetry adapted in the sense that the *translational* symmetry has been fully exploited in employing this basis. Thus, the full crystal orbital problem is divided into separate problems for each wave vector $\vec{k}$, each problem being of the dimension of the number of atomic orbitals per unit cell. Because of the periodicity of $e^{i\vec{k}\cdot\vec{R}}$ (with respect to $\vec{k}$ in this context), one may restrict oneself to the first Brillouin zone in $\vec{k}$ space. Further details on these matters can be found in standard texts.[15]

We have already discussed the expectations we have for the crystal electronic structure and bonding in terms of the MO's of the $Mo_6S_8$ cluster. The most natural way to decompose the crystal orbitals, then, would be in terms of the $Mo_6S_8$ cluster orbitals.

(15) See, for example: (a) Harrison, W. A. "Solid State Theory"; Dover: New York, 1980. (b) Ashcroft, N. W.; Mermin, N. D. "Solid State Physics"; Holt, Rinehart and Winston, New York, 1976.

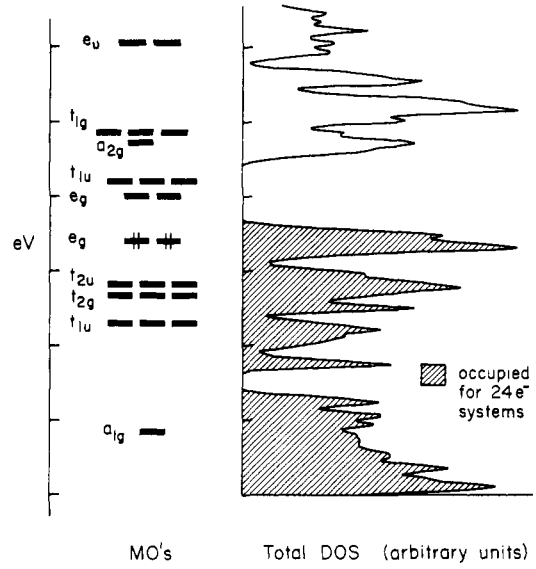


**Figure 5.** Molybdenum-based MO's for the $Mo_6S_8^{4-}$ cluster and the total density of states curve for an $Mo_6S_8$ crystal.

In principle we could prepare a set of Bloch basis orbitals ($\Phi_\alpha(\vec{k})$) from the set of cluster *molecular* orbitals ($X_\alpha$):

$$\Phi_\alpha(\vec{k}) = \frac{1}{N^{1/2}}\sum_{\vec{R}} e^{i\vec{k}\cdot\vec{R}} X_\alpha(\vec{r} - \vec{R}) \tag{2}$$

The *crystal* orbitals ($\psi_n(\vec{k})$) ($n$ is the band index which runs from one to the number of basis functions per unit cell) may be equally well written as linear combinations of the AO Bloch basis orbitals ($\phi_\mu(\vec{k})$) or as MO Bloch basis orbitals ($\Phi_\alpha(\vec{k})$):

$$\psi_n(\vec{k}) = \sum_\mu c_{\mu n}(\vec{k})\phi_\mu(\vec{k}) \tag{3a}$$

$$\psi_n(\vec{k}) = \sum_\alpha d_{\alpha n}(\vec{k})\Phi_\alpha(\vec{k}) \tag{3b}$$

where the $\vec{k}$ dependence of the coefficients in these equations is to be noted. The coefficients in (3a) and (3b) may be related via the molecular orbital wave functions:

$$X_\alpha = \sum_\mu b_{\mu\alpha}\chi_\mu \tag{4a}$$

which directly gives, using definitions 1 and 2

$$\Phi_\alpha(\vec{k}) = \sum_\mu b_{\mu\alpha}\phi_\mu(\vec{k}) \tag{4b}$$

Finally, from (3a), (3b), and (4b) we obtain

$$d_{\alpha n}(\vec{k}) = \sum_\mu (b^{-1})_{\alpha\mu} c_{\mu n}(\vec{k}) \tag{5}$$

which gives a prescription for obtaining the ($\vec{k}$ dependent) crystal orbital coefficients in terms of MO's from those in terms of AO's.

The above merely makes formal the crystalline counterpart to the fragment molecular orbital approach, a powerful conceptual tool for understanding complicated molecules in terms of simpler fragments.[16] Having thus armed ourselves, we can proceed to extract from the total density of states for the Chevrel phase compounds the contributions of each of the molecular orbitals discussed earlier. Extended Hückel band structure calculations were carried out on a $Mo_6S_8$ system in which an ideal $O_h$ cluster was used (intracluster Mo–Mo = 2.705 Å and Mo–S = 2.46 Å).

(16) (a) Elian, M.; Hoffmann, R. *Inorg. Chem.* **1975**, *14*, 1058–1076. (b) Thorn, D. L.; Hoffmann, R. *Ibid.* **1978**, *17*, 126–140. (c) Schilling, B. R.; Hoffmann, R. *J. Am. Chem. Soc.* **1979**, *101*, 3456–3467. (d) Burdett, J. K. "Molecular Shapes"; Wiley: New York, 1980. (e) Mingos, D. M. P. *Adv. Organomet. Chem.* **1977**, *15*, 1–51; *MTP Int. Rev. Sci.: Phys. Chem., Ser. Two* **1975**, *11*, 121; *Nature (London), Phys. Sci.* **1972**, *236*, 99–102. (f) Hoffmann, R. *Angew. Chem.* **1982**, *94*, 725–739.

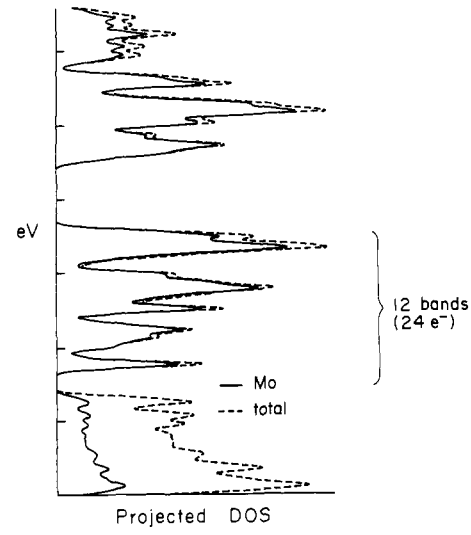


**Figure 6.** Molybdenum contribution to the total DOS is shown. The separation between "Mo orbitals" and "S orbitals" is apparent. The total DOS is shown for reference.

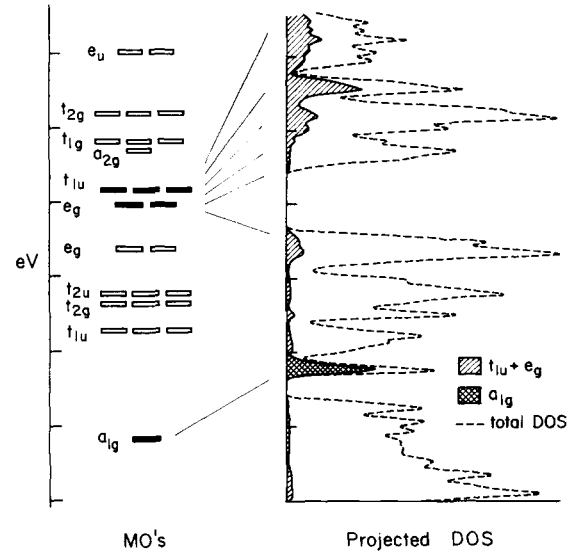


**Figure 7.** Projected DOS curves for the "$z^2$ type" orbitals of the $Mo_6S_8$ unit are shown. The MO's of the cluster and the total DOS for the crystal are included for reference.

The rhombohedral lattice constant was taken to be 6.544 Å, the rhombohedral angle was 90°, and the "turn angle" discussed in reference to **4** was taken as 25°. The geometry leads to intercluster Mo–S = 2.51 Å and Mo–Mo = 3.25 Å. Density of states (DOS) curves were obtained following a calculation including 53 $\vec{k}$ points in the irreducible wedge of the rhombohedral Brillouin zone and smoothing of the results obtained with Gaussian functions with a half-width of 0.083 eV. Further details are to be found in the Appendix.

In Figure 5 we show the total DOS curve for the $Mo_6S_8$ crystal. At left in the figure are the molecular orbitals for the cluster with the electron filling appropriate for a 24 cluster electron system. The shaded region in the DOS indicates the filled levels for a 24-electron system also. The 0.8-eV gap see above the 24-electron level is consistent with the semiconducting behavior reported for these systems and mentioned earlier.

In Figure 6 we show the total Mo contribution to the DOS obtained from a Mulliken population analysis of the crystal orbitals. The solid line gives the Mo DOS and the dotted line is the total DOS, included for comparison (the difference, of course, is the sulfur contribution to the density of states). The 24 cluster Mo electrons can be roughly said to occupy 12 bands which comprise the 2-eV-wide block indicated in Figure 6. Note the

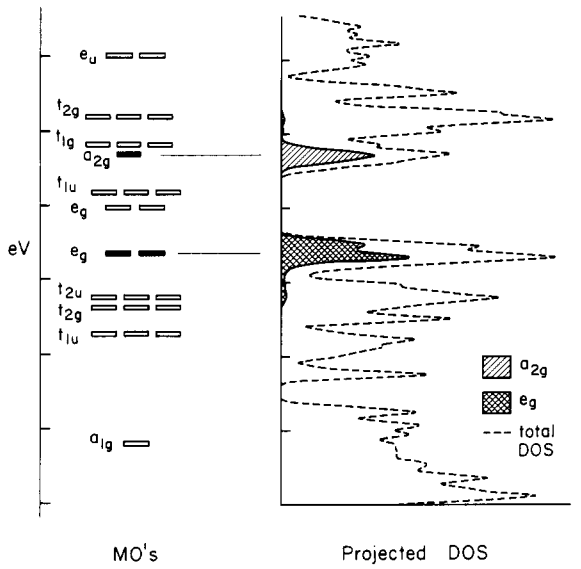


**Figure 8.** Orbitals with "δ pseudosymmetry" are projected. The cluster MO's and the total crystal DOS is included for reference.

small sulfur contribution to these bands.

Using the methods described earlier in this section, we may directly trace the fate of the cluster orbitals after "crystallization" by performing population analysis on the crystal orbitals and projecting out the various cluster molecular orbital contributions. We are particularly interested in the LUMO $e_g$ and $t_{1u}$ orbitals as well as the lowest Mo $a_{1g}$ orbital since these orbitals are those which we supposed would be involved in bonding to chalcogens on neighboring clusters. In Figure 7 we have projected out the contributions of these MO's. The perturbation of the LUMO orbitals ($t_{1u}$ and $e_g$) is pronounced; the orbitals are pushed up as in the cluster model calculation and they clearly "spread out" in energy. The spreading of these orbital contributions is indicative of the loss of the molecular "identity" of the $e_g$ and $t_{1u}$ LUMO orbitals. The $a_{1g}$ Mo bonding orbital is also pushed up but gives rise to a very narrow peak in the projected DOS for this MO. The narrowness of this peak can be explained in terms of a significant increase in Mo p hybridization into the $a_{1g}$ orbital, which serves to localize this orbital more on the "inside" of the cluster. This p hybridization, illustrated in **11**, is induced by chalcogen donor

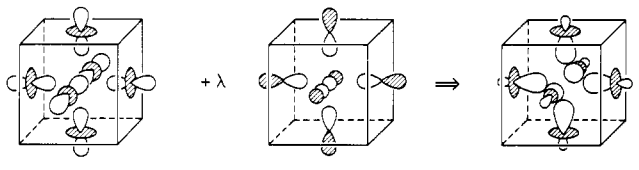


**11**

orbitals of neighbor clusters and shows up upon examination of the crystal orbital wave functions at various $\vec{k}$ points.

In the discussion of the $Mo_6S_8$ cluster we also put emphasis upon the $e_g$ HOMO and an $a_{2g}$ orbital (see **10**) which were said to display "δ pseudosymmetry" in reference to their overlap with chalcogen atoms which cap the square faces of the cluster. Figure 8 shows the projected DOS for these MO's, confirming our statements about these orbitals giving rise to narrow bands. It can be seen that to a significant extent the crystal orbitals at the top of the valence band and the bottom of the conduction band are composed of $x^2 - y^2$ type orbitals and that the "molecular orbital" integrity of these levels is preserved. It should be noted that the double peaked nature of the $e_g$ (HOMO) DOS was first predicted by Andersen[14b] in a model which ignored mixing with other cluster MO's.

A comparison of various bond strengths (e.g., intracluster Mo–S vs. intercluster Mo–S) may be gleaned from overlap populations derived from our band structure results. Examination of the Mulliken charges also provides information about expected substitution patterns in mixed systems (e.g., where do we expect sulfur atoms to locate in $MMo_6Se_{8-x}S_x$?). Since atomic charges, overlap populations, and the total energy are all quantities which are obtained by Brillouin zone integrations (i.e., are derived as averages of periodic functions in $\vec{k}$ space), we may get increasingly good estimates of these quantities by using "special points" schemes[17] devised for getting such averages. The basic idea of the special points method is to use one or a small number of $\vec{k}$ points to precisely estimate averages of $\vec{k}$ dependent quantities. While we will not herein describe in detail how this is done, it suffices to say that the precision of these estimates may be checked by comparing results from a small set of points with those of a larger set; if averages are not significantly changed, then one may be confident of the precision of the numbers obtained. In our calculations on the $Mo_6S_8^{4-}$ system (i.e., with the formal cluster electron count at 24), we used two-point and twelve-point sets, obtaining excellent convergence of the averages—results quoted below are completely unchanged in using the smaller and larger point sets (these point sets are given in the appendix). In **12** we

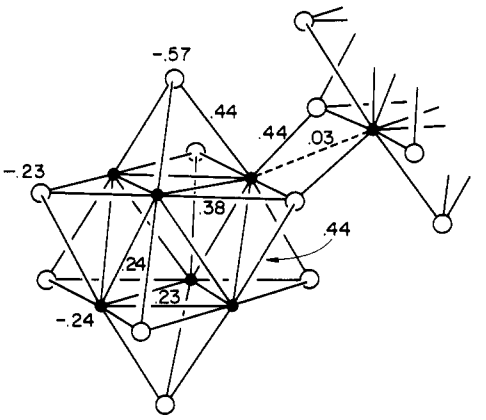


**12**

have displayed the overlap populations for symmetry unique bonds and the atomic charges.

Of the quantities shown in **12**, only the charge on the Mo atoms will vary strongly as the electron count is lowered from 24 (i.e., Mo is oxidized). Since oxidation removes electrons from Mo bonding orbitals (largely from the $e_g$ HOMO), there would be moderate overall Mo–Mo bond weakening. In a free $Mo_6S_8^{4-}$ cluster there are only two overlap populations to consider: Mo–Mo = 0.23 and Mo–S = 0.45. A comparison with **12** reveals two significant changes upon crystallization (aside from the obvious formation of intercluster bonds): (1) One type of intracluster Mo–S bonds shows a fairly large decrease in the overlap population from 0.45 to 0.38. (2) Sulfurs involved in intercluster bonding show a marked lowering of charge from −0.59 to −0.23 which is accompanied by a compensating change in the Mo charge from +0.11 to −0.24 upon crystallization. The first effect may be understood in terms of a trans effect resulting from the intercluster Mo–S bonding (see **12**). The second effect may be seen as a result of the dative donation from sulfur to molybdenum on the neighboring cluster. The charge assymetry on chalcogen atoms indicates that in mixed compounds, $MMoSe_{8-x}S_x$, sulfur atoms should prefer the sites on the 3-fold axis. This agrees with results of Delk and Sienko[18] and more recent work of Johnson and Sienko.[19] Earlier work of Lin and Burdett[6a] predicts a charge assymetry opposite that of the present work. It could be that omission of the Mo d orbitals in that work is responsible for this

(17) (a) Baldareschi, A. *Phys. Rev. B: Solid State* **1973**, *B8*, 5212–5215. (b) Chadi, D. J.; Cohen, M. L. *Ibid.* **1973**, *B8*, 5747–5753. (c) Chadi, D. J. *Ibid.* **1977**, *B16*, 1746–1747. (d) Monkhorst, H. J.; Pack, J. D. *Ibid.* **1976**, *B13*, 5188–5192. (e) Pack, J. D.; Monkhorst, H. J. *Ibid.* **1977**, *B16*, 1748–1749.

(18) Delk, F. S.; Sienko, M. J. *Inorg. Chem.* **1980**, *19*, 1353–1356.

(19) Johnson, D.; Sienko, M. J., private communication.

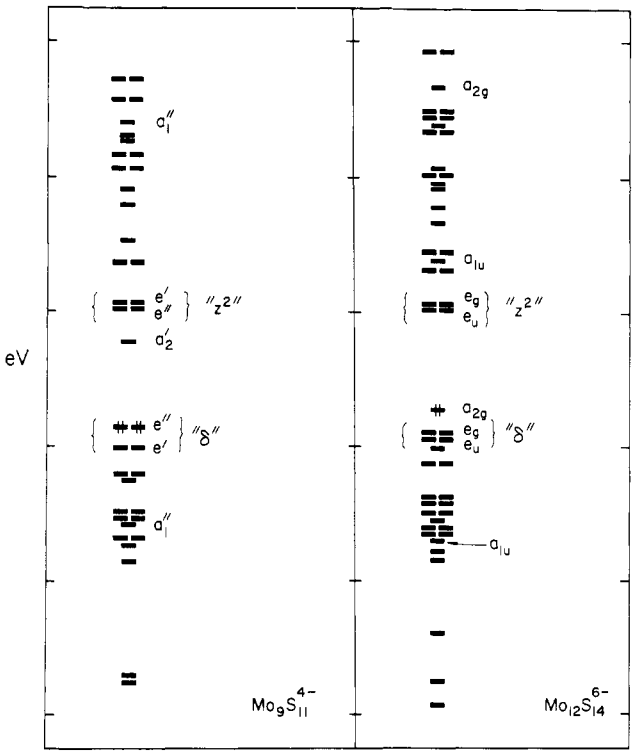


**Figure 9.** Molecular orbital diagrams for $Mo_9S_{11}^{4-}$ and $Mo_{12}S_{14}^{6-}$. Labeled levels are discussed in the text.

difference. The question of halogen site preference in compounds such as $Mo_6S_6Br_2$ and $Mo_6Se_{8-x}Br_x$ ($0 \leq x \leq 3$) probably has as much to do with the anion coordination number as the charge distribution. Since the chalcogens bonded to neighboring clusters are best viewed as fully four-coordinate (in view of **12**), one would expect that halogens would prefer the lower coordinate 3-fold sites—again in agreement with experimental indications.[20]

### The $Mo_9X_{11}$ and $Mo_{12}X_{14}$ Clusters

We have seen in some detail how structure and bonding in the $Mo_6X_8$ systems may be understood in terms of the isolated $Mo_6X_8$ clusters and their molecular orbitals. In this section we will investigate $Mo_9X_{11}$ and $Mo_{12}X_{14}$ clusters and from the cluster molecular orbitals make inferences about intercluster bonding and other matters based upon our experience with the $Mo_6X_8$ prototype.

Because of the increasing complexity one faces in understanding the large number of molecular orbitals which result from calculations on these larger systems, we will be sparing in detail and present only the more important features. In particular we shall emphasize those features which serve to unify our thinking about the series of compounds $Mo_nX_{n+2}$ ($n$ = 2, 3, 4, ... $\infty$).

Before proceeding with a molecular orbital analysis for the compounds containing $Mo_9X_{11}$ and $Mo_{12}X_{14}$ clusters, it is most useful to make explicit the electron counting schemes for these compounds. For the $Mo_9X_{11}$ systems, several compounds have been prepared,[2b,7,8] including $In_{\sim 3}Mo_{15}Se_{19}$ [$=In_xIn_2(Mo_6Se_8)(Mo_9Se_{11})$ with $0.9 < x < 1.4$], $M_2Mo_{15}Se_{19}$ [$=M_2(Mo_6Se_8)(Mo_9Se_{11})$ with M = K, Ba, In, Tl], and $M_2Mo_{15}S_{19}$ [$=M_2(Mo_6S_8)(Mo_9S_{11})$ with M = K, Rb, Cs]. If we assign all the cations except Ba an oxidation state of 1+ (Ba, of course, being 2+) and further assume that the formal electron count on the $Mo_6X_8$ clusters in these materials is between 20 and 24 (as in the "unmixed" $Mo_6X_8$ systems), then the formal metal electron count on the $Mo_9X_{11}$ clusters will be between 30 and 36 for the compounds listed. A more reasonable value would lie somewhere between these extremes since the extreme values imply complete charge transfer from one cluster type to the other. Compounds containing $Mo_{12}X_{14}$[2b,7,9] units include $M_2Mo_9S_{11}$ [$=M_4(Mo_6S_8)(Mo_{12}S_{14})$ with M = K, Tl]. With the same assumptions as before, the $Mo_{12}X_{14}$ cluster electron count for these compounds will be between 44 and 48.

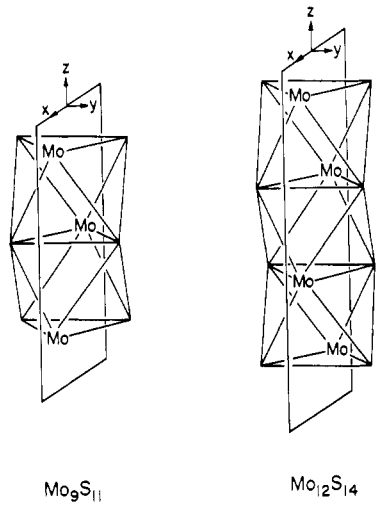


**Figure 10.** Molecular planes for the contour plots of Figures 11 and 12. The intersection of these planes with the Mo atoms of the $Mo_9$ and $Mo_{12}$ skeletons of the $Mo_9X_{11}$ and $Mo_{12}X_{14}$ clusters is shown. The Cartesian axes should be noted.

In Figure 9, we show molecular orbital diagrams for $Mo_9S_{11}^{4-}$ and $Mo_{12}S_{14}^{6-}$ clusters with 36 and 50 cluster electrons, respectively. The electron count has been chosen to produce a closed-shell configuration for each cluster and conforms approximately to the ranges discussed above for real systems. In what follows we will limit discussion only to levels which have been given symmetry labels in Figure 9 but remark that there is clear separation between metal–metal bonding and antibonding levels. The electron counts found in the systems observed so far are nearly optimal in that Mo–Mo bonding levels are nearly all filled.

Turning to the frontier orbitals for these clusters, in Figure 9 we have labeled orbitals for both $Mo_9S_{11}$ and $Mo_{12}S_{14}$ as "$\delta$" and "$z^2$". The $z^2$ type orbitals are displayed schematically in **13** for the $Mo_{12}S_{14}$ cluster. As **13** implies, these orbitals are quite

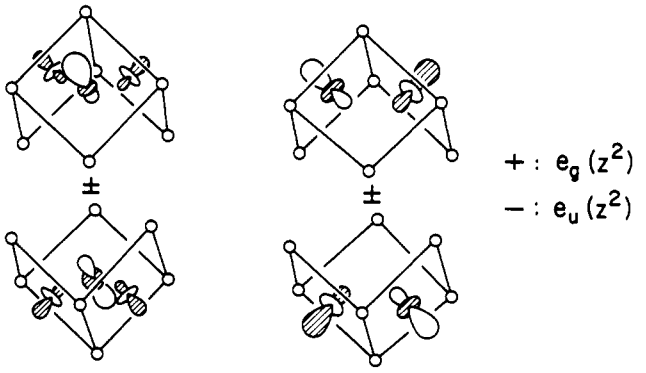


**13**

localized on the "terminal" Mo atoms at the ends of the clusters (i.e., on the Mo atoms which are locally square planar with respect to sulfur coordination). The reason for our "$z^2$" label is also clear: if we consider each terminal Mo to reside at the origin of a local coordinate system in which the $z$ axis is normal to the square face in question, then these orbitals are aptly described as having $z^2$ character with some s and p hybridization. Thus, we find that the $Mo_9S_{11}$ and $Mo_{12}S_{14}$ clusters share with $Mo_6S_8$ the characteristic of having low-lying unoccupied orbitals which project from the Mo atoms in the square faces of the cluster. Figures 11 and 12 display orbital contour plots from each of the $z^2$ type orbitals of $Mo_9S_{11}$ and $Mo_{12}S_{14}$, respectively. (Figure 10 shows the molecular symmetry planes in which the contours are plotted. Figures 11 and 12 show one member of the degenerate e′, e″ and $e_g$, $e_u$

(20) Sergent, M.; Fischer, Ø.; Decroux, M.; Perrin, C.; Chevrel, R. *J. Solid State Chem.* **1977**, *22*, 87–92.

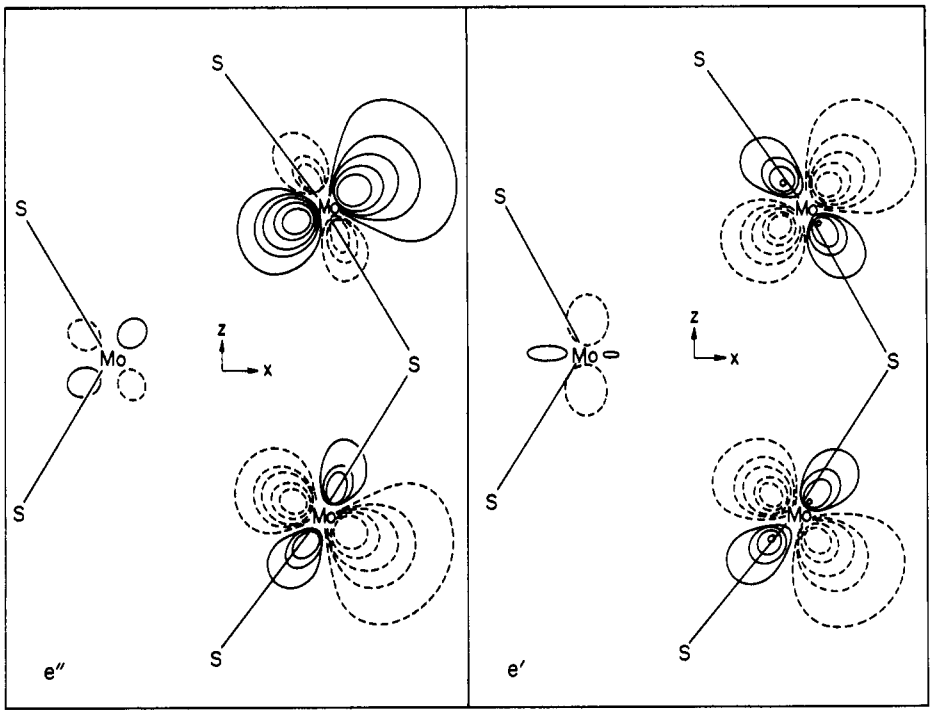


**Figure 11.** Contour plots of the "$z^2$ type" orbitals of $Mo_9X_{11}$ are displayed. The three Mo atoms which appear are those which are at left in Figure 10. Contour values are as in Figure 3.

orbitals of $Mo_9S_{11}$ and $Mo_{12}S_{14}$.) The obvious consequences of these orbitals is that there exists for the larger cluster systems a strong driving force for packing in the solid state so as to form Mo–S intercluster bonds—just as in the $Mo_6S_8$ systems.

The similarity between the $Mo_6S_8$ orbitals and those for the larger clusters extends to the HOMO's for these systems also. Indeed, the orbitals labeled as "$\delta$" in Figure 9 bear a strong resemblance to $e_g$ HOMO orbitals of $Mo_6S_8$. For $Mo_{12}S_{14}$ we may schematically depict the $e_g$ and $e_u$ "$\delta$" orbitals as in **14**. These

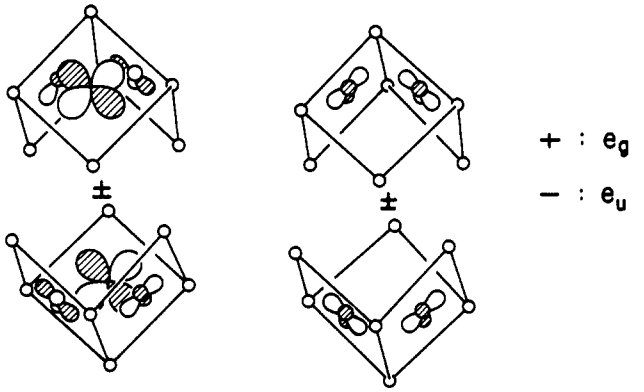


**14**

orbitals present a $\delta$ overlap to chalcogens which cap the square faces of the clusters. As a result, we expect these orbitals to be negligibly perturbed upon the formation of intercluster Mo–S bonds—despite the fact that the $\delta$ type orbitals on $Mo_9S_{11}$ and $Mo_{12}S_{14}$ are quite localized on the terminal Mo atoms.

In the $Mo_6S_8$ system, qualitative understanding of intercluster bonding was extractable by considering a model in which six $S^{2-}$ ions were placed over the square faces of the cluster and the perturbation of the cluster Mo orbitals was analyzed. Figures 13 and 14 show the results of calculations in which 6 $S^{2-}$ cap the faces of the $Mo_9S_{11}$ and $Mo_{12}S_{14}$ clusters. Orbitals in the bonding and antibonding blocks are only weakly perturbed by interaction with the capping sulfides. As one would expect, it is the $z^2$ type orbitals which are pushed up by the added donors, confirming that the intercluster bonding in the $Mo_9X_{11}$ and $Mo_{12}X_{14}$ systems is basically the same as in the $Mo_6X_8$ system. Also expected is the very weak perturbation of the $\delta$ type HOMO's seen in these diagrams. As in the $Mo_6S_8$ systems, we expect that the levels near the Fermi level will retain their molecular character due to the poor overlap of $\delta$ type orbitals with orbitals in neighboring clusters. The existence of such localized levels at the Fermi level agrees well with conjectures put forward to explain the high critical fields necessary to extinguish the superconductivity[8] in the $In_{\sim 3}Mo_{15}Se_{19}$ systems. It is likely that since $\delta$ type orbitals will not overlap with AO's centered upon the capping chalcogens in these systems, the intercluster Mo–Mo distance may be important in determining *electronic properties* of all the cluster materials even though *structural characteristics* are determined by Mo–X intercluster bonding.

Before considering other matters, we should note that there appears to be an interesting connection between the frontier orbitals we have discussed for the larger clusters and the concept of "surface states" commonly used by surface scientists.[21] The characterization of the $z^2$ type orbitals as surface states is reasonable on several grounds: (a) The orbitals are quite localized upon the terminal Mo atoms (i.e., on the ends or "surface") of the developing chains of $Mo_3X_3$ units. (b) The orbitals are separated in energy from the blocks of bonding and antibonding cluster orbitals (as it turns out, the $z^2$ type orbitals lie in a gap in the band structure of $(Mo_3X_3)_\infty^-$ chains, making them "gap" states; see below). (c) The splitting between the $e_g$ and $e_u$ combinations of $z^2$ hybrids in $Mo_{12}S_{14}$ is very small—consistent with small electronic coupling between the ends of the cluster. (d) The orbital hybridization of the $z^2$ type orbitals apparent in Figures 11 and 12 is clearly evocative of "dangling bonds" as is the fact that these clusters all form Mo–X intercluster bonds, using these hybrids. All of the factors provide convincing evidence that these $z^2$ type end states should persist in chains of any length (calculations on the hypothetical system $Mo_{15}S_{17} = S(Mo_3S_3)_5S$ yield $z^2$ type hybrids which are virtually identical in energy and extent of localization with the orbitals found in $Mo_{12}S_{14}$).[22] Factors (a),

(21) See, for example: "The Nature of the Surface Chemical Bond"; Rhodin, T. N., Ertl, G., Eds.; North Holland: Amsterdam, 1979.

(22) Note that an approach which concentrates on charge densities alone will miss these "dangling bonds" since the levels we are concerned with are not occupied.

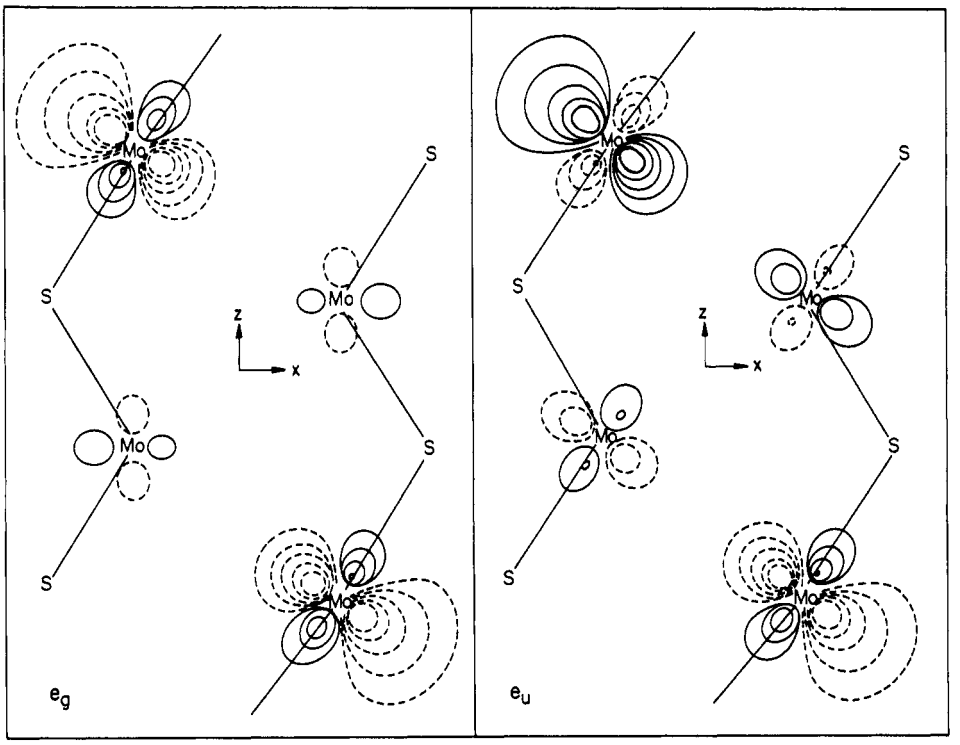


**Figure 12.** Contour plots of the "$z^2$ type" orbitals of $Mo_{12}X_{14}$ are displayed. The four Mo atoms which appear are those which are at right in Figure 10. Contour values are as in Figure 3.

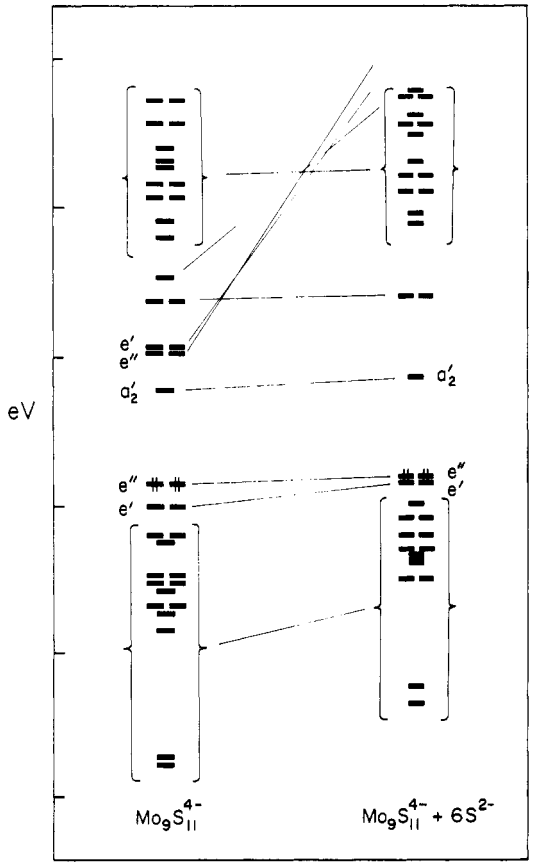


**Figure 13.** Perturbation of the $Mo_9X_{11}^{4-}$ levels by six capping $S^{2-}$ ions.

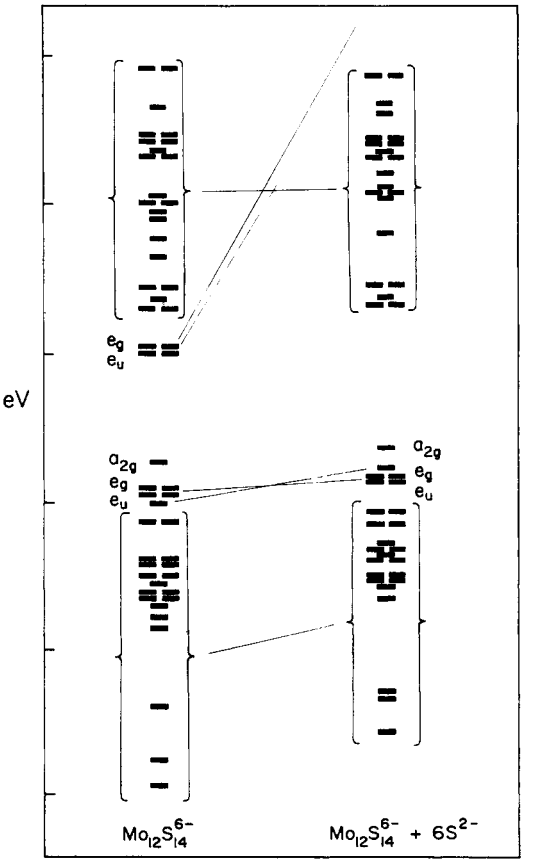


**Figure 14.** Perturbation of the $Mo_{12}X_{14}^{6-}$ levels by six capping $S^{2-}$ ions.

(b), and (c) above apply to the $\delta$ type orbitals as well. Since these orbitals will presumably be important in transport properties, the question of whether there is appreciable coupling between the **ends** of a given cluster as well as between clusters is intriguing.

Speaking generally, Figures 13 and 14 allow us to make predictions about what electron counts serve to give a closed-shell electronic structure for these clusters, or alternatively, we can predict how many electrons will be needed to get a semiconducting crystal for these systems. For a $Mo_{12}X_{14}$ cluster we should find that a 50-electron cluster system (or a 74-electron mixed $Mo_{12}X_{14}$–$Mo_6X_8$ system) is semiconducting. The $Mo_9X_{11}$ systems are more problematic; if the $a_2'$ orbital in the "gap" can be ignored

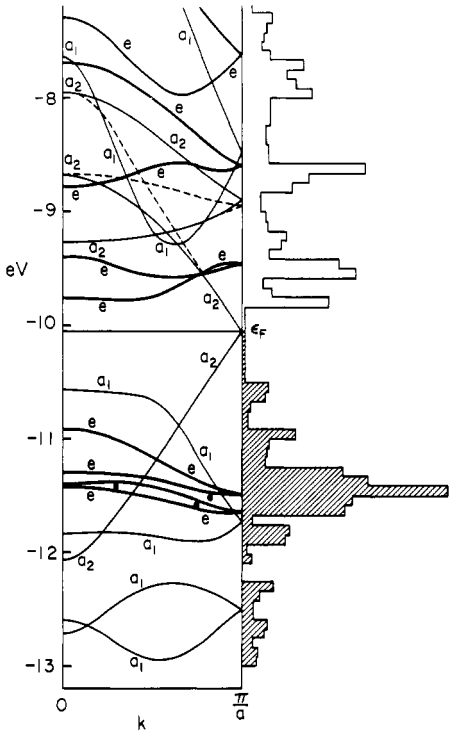


**Figure 15.** Band structure and total DOS for $(Mo_6S_6^{2-})_\infty$ chain is shown. Shaded levels in the DOS are occupied for systems with 13 electrons per $Mo_3S_3$ unit.

(i.e., is not occupied) then a 36-electron system will have a closed shell; if not, we need 38 electrons. Correspondingly, mixed $Mo_9X_{11}$–$Mo_6X_8$ systems will "hold" up to 60 or perhaps 62 electrons.

Up until now, we have ignored the $a_2'$ orbital just referred to. What is the nature of this orbital? Why is this level encountered in $Mo_9S_{11}$ but not in $Mo_6S_8$ or $Mo_{12}S_{14}$? The answer to these questions is intimately connected to the most interesting feature in the electronic structure of the $(Mo_3X_3^-)_\infty$ chain compounds.

### The Infinite Limit: $(Mo_3X_3^-)_\infty$

In an earlier communication[23] we noted that there is a clear separation between Mo–Mo bonding and antibonding levels in an $(Mo_3X_3^-)_\infty$ chain—as can be seen by inspection of Figure 15, where we show the Mo band structure and DOS for the $(Mo_3S_3^-)_\infty$ one-dimensional chain. This Mo–Mo bonding–antibonding separation, a feature common to all the systems we've seen, probably contributes significantly to their thermodynamic stability. As can be seen, a metal electron count of 13 electrons per $Mo_3S_3$ unit is optimal in that the bonding levels are filled and the antibonding levels are empty. In our calculations for this chain we deliberately set in-plane and out-of-plane Mo–Mo distances equal to 2.705 Å to compare calculated overlap populations (see **9**). (Earlier work on $(Mo_3Se_3^-)_\infty$ used experimental structural parameters.) In agreement with observed bond length differences (in-plane bonds shorter than out-of-plane bonds), the overlap populations between Mo atoms within the $Mo_3S_3$ triangles were appreciably larger than interplane Mo–Mo overlap populations (0.29 vs. 0.23).

Perhaps the most convenient way of understanding the $(Mo_3S_3^-)_\infty$ Mo bands is in terms of the Mo molecular orbitals of the $Mo_3S_3$ fragment, shown in Figure 16. While it would take us too far afield to rationalize the levels in detail, the ordering shown is plausible in terms of Mo–Mo bonding and Mo–S antibonding interactions. We will analyze the band structure in Figure 15 by using the $C_{3v}$ symmetry labels—as we have done at right in Figure 16 for the $Mo_3S_3$ fragment orbitals. This is appropriate because among the point group operations for the chain only the $C_3$ axis and the vertical mirror planes[24] leave the

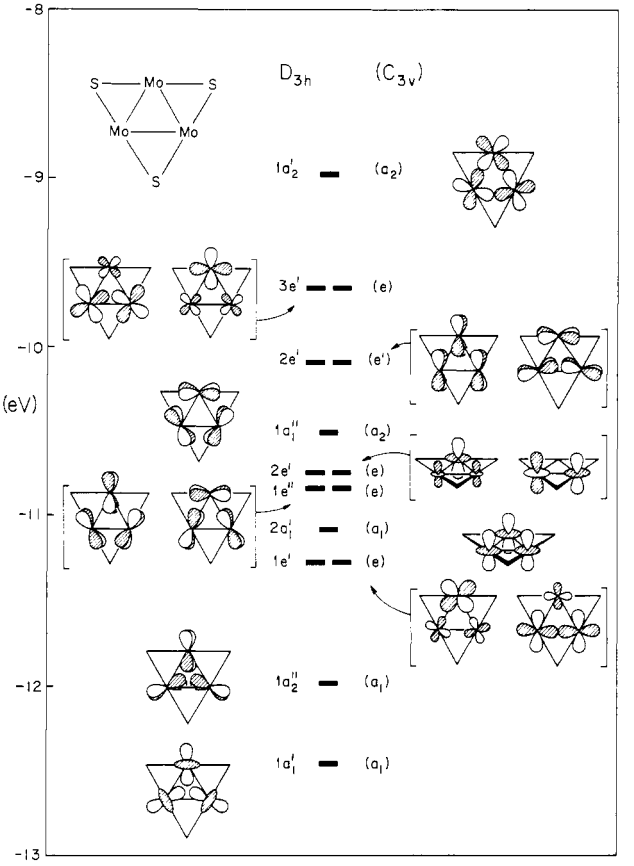


**Figure 16.** Molecular orbitals for the $Mo_3S_3$ fragment.

wave vector $\vec{k}$ unaltered for all $\vec{k}$ (the horizontal mirror planes carry $\vec{k}$ to $-\vec{k}$; for details, see ref 25). It should be noted that a $6_3$ screw axis is coincident with the 3-fold chain axis (there are two chemically equivalent $Mo_3S_3$ units per unit cell) which explains the "folded" nature of the bands in Figure 15 and the crossings between bands with identical symmetry labels. It is simplest to consider each folded band as a single band; this yields 15 bands—allowing for the five doubly degenerate e bands—in correspondence with the 15 levels of the $Mo_3S_3$ unit.

We discuss the chain band structure by considering each symmetry type in turn: $a_1$, e, and $a_2$ (recall, we are using $C_{3v}$ labels).

**$a_1$ Bands**: Of the three $a_1$ fragment orbitals shown in Figure 16, the lowest—an in-plane bonding combination of "$z^2$" type orbitals—is least perturbed upon stacking of the fragments into a chain. This orbital contributes appreciably only to the lowest $a_1$ band and lower part of the second $a_1$ band. The other two $a_1$ fragments, composed as they are of orbitals which project out of the plane of the $Mo_3$ triangle, overlap well with the corresponding orbitals of neighboring fragments. Hybridization between these two fragment orbitals is responsible for a strongly avoided crossing in the upper two $a_1$ bands. This mixing contributes to interplanar Mo–Mo bonding and the gap between the second and third $a_1$ bands plays an important role in the electronic and structural characteristics of the $(Mo_3X_3^-)_\infty$ chains, as we discuss below.

**e Bands**: As it turns out, interplanar overlaps among e type fragment orbitals are smaller than the $a_1$ type overlaps. As a result the e bands are narrower, though the complicated form of these bands is a result of hybridization among the various fragment orbitals (especially for the upper three e bands). Notably, a gap

(23) Hughbanks, T.; Hoffmann, R. *Inorg. Chem.* **1982**, *21*, 3578–3580.

(24) In the actual structures the vertical mirror planes are not present. Our inclusion of the mirror planes does not affect results quoted—only a weak mixing between $a_1$ and $a_2$ orbitals is introduced by removing the mirror plane by distorting the chains slightly to observed geometries.

(25) See, for example: (a) Tinkham, M. "Group Theory and Quantum Mechanics"; McGraw-Hill: New York, 1964; Chapter 8. (b) Lax, M. "Symmetry Principles in Solid State and Molecular Physics"; Wiley: New York, 1974.

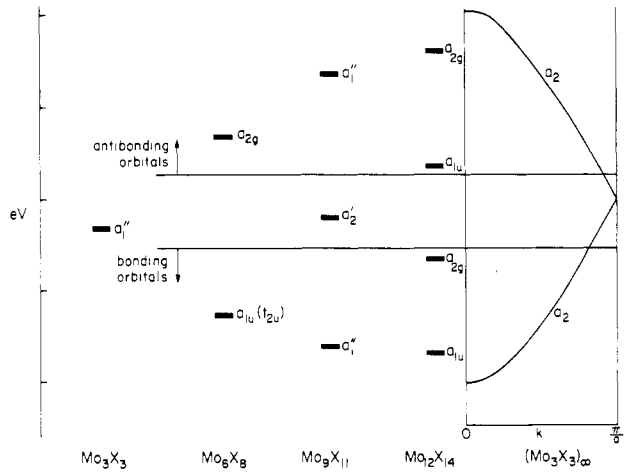


**Figure 17.** Schematic representation of the orbitals derived from the $a_1''$ fragment orbital of $Mo_3X_3$ in each of the systems studied in this paper.

in the e type bands is observable near the Fermi energy.

**$a_2$ Bands**: Simplest, yet most intriguing, are the bands built up from the $a_2$ type fragment orbitals. The upper of the two $a_2$ fragment orbitals is made up of in-plane d orbitals and hence, were it not for mixing with the band from the lower fragment, would give rise to a narrow (~0.5 eV) band. As illustrated in **15**,

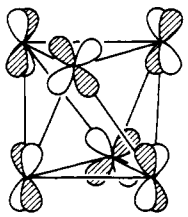

**15**

however, overlap between the lower $a_2$ $Mo_3S_3$ orbitals on adjacent fragments is relatively large and thus the band derived from this MO is comparatively wide (~4 eV; the dotted lines in Figure 15 illustrate the hypothetical bands as they would appear if the two $a_2$ MO's did not interact). This wide $a_2$ band is the only one which spans the gap between bonding and antibonding Mo orbitals. Not surprisingly then, this band is half-occupied for the compounds synthesized so far (which have 13 Mo electrons per $Mo_3X_3$ unit).

The presence of the single $a_2$ band crossing the Fermi level has a number of implications. The possibility that the $(Mo_3X_3^-)_\infty$ chains will undergo a Peierls distortion (pairing distortion) due to the half-filled $a_2$ band was discussed in our earlier report and by Kelly and Andersen.[26] There is also the possibility that the absorption spectrum will show some interesting polarization effects because of various selection rules that are operative for direct transitions in this relatively high-symmetry system. Note also that the $a_2$ band is of different rotational symmetry than the cluster "surface states" ($z^2$ type orbitals) discussed earlier which are of e symmetry. These e type orbitals lie in a gap between e bands for the chain systems; this justifies our calling these orbitals "gap" states even though no band gap appears in Figure 15.

An analysis of the cluster electronic structure (of $Mo_6X_8$, $Mo_9X_{11}$, $Mo_{12}X_{14}$) in terms the $Mo_3X_3$ fragment and "capping" X atoms would likely be complex, tedious, and uninformative. However, the $a_1''$ fragment orbital (with the $D_{3h}$ label) is rather unique, and it proves quite simple to find and understand the levels of the clusters derived from this fragment orbital. Indeed, the developing $a_2$ band can be identified and is shown schematically in Figure 17 (We neglect the contribution of the $a_2'$ $Mo_3X_3$ fragment orbital).

(26) (a) Kelly, P. J.; Andersen, O. K. In "Superconductivity in d- and f-Band Metals", Sohl, H.; Maple, M. B., Eds.; Academic Press: New York, 1982, pp 137–140. (b) Nohl, H.; Andersen, O. K. *Ibid.* pp 161–165.

**Table I.** Closed-Shell Electron Counts for $Mo_nX_{n+2}$ Systems

| | |
|---|---|
| $Mo_6X_8$ | 24 |
| $Mo_9X_{11}$ | 36–38? |
| $Mo_{12}X_{14}$ | 50 |
| $(Mo_3X_3)_\infty$ | 13 per $Mo_3X_3$ |

A few comments about the specific levels shown in Figure 17 are in order. First of all, the picture is most "schematic" for $Mo_6X_8$. The lower $a_{1u}$ orbital is not unique and actually descends from the $t_{2u}$ set (see Figure 1). Also, the $a_{2g}$ orbital for $Mo_6X_8$ has considerable contribution from the neglected $a_2'$ $Mo_3X_3$ fragment orbital—in fact this orbital has been discussed earlier and appears in **10** (a view down a 3-fold body axis of the cube will betray its "$a_2$" character). The $a_2'$ orbital which appears in the bonding–antibonding gap for $Mo_9S_{11}$ is seen to be merely the nonbonding combination of the $Mo_3S_3$ $a_1''$ fragment orbitals, as shown in **16**. A "chain" with an *odd* number of $Mo_3S_3$ fragments

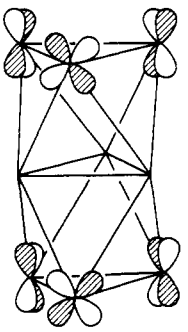

**16**

would be expected to exhibit a nonbonding orbital in the bonding–antibonding gap. $Mo_6S_8$ and $Mo_{12}S_{14}$, being composed of an *even* number of $Mo_3S_3$ fragments, do not have such a nonbonding $a_2$ type orbital. Finally, the $a_2$ HOMO of $Mo_{12}S_{14}$, which we summarily ignored previously, is also descended from the $a_1''$ fragment orbital.

Let us recapitulate on the matter of "closed-shell" electron counts for the systems we have studied. In Table I we have listed our results. Simplistically, we may say that $Mo_9X_{11}$ is "satisfied" with 37 electrons (after all, the $(Mo_3X_3^-)_\infty$ chain has a half-filled $a_2$ band!). Loosely speaking then, it appears that for each $Mo_3X_3$ unit added, 13 more electrons can be added—which is entirely consistent with the 13 electrons per $Mo_3X_3$ seen for the $(Mo_3X_3^-)_\infty$ chains. Of course, the specifics of each of the systems must be borne in mind: systems with an odd number of $Mo_3X_3$ units may not show closed-shell characteristics (e.g., there may be no semiconducting electron count); the counting scheme given merely suggests an optimal electron count. Obviously, one may find fewer electrons in any given system, and indeed it is these electron deficient systems which will have interesting conducting properties.

### Other Compounds and Concluding Remarks

For ease of exposition and because of the myriad of interconnections between the various molybdenum chalcogenide compounds, we have concentrated on these systems to the exclusion of other interesting materials. There are, however, several systems where our results can be seen to be relevant.

Clusters which are isoelectronic to $Mo_6S_8^{4-}$ have long been known. $Mo_6Cl_8^{4+}$, first found in crystal compounds $[Mo_6Cl_6](OH)_4 \cdot 8H_2O$[27] and $(NH_4)_2[Mo_6Cl_6]Cl_6 \cdot 2H_2O$,[28] is bonded to ligands so as to cap the square faces of the cluster. Thus, although there is no intercluster bonding as in the Chevrel phases, the electronic requirements of the basic structural unit are satisfied in fundamentally the same fashion. Clusters characterized as $Re_6S_8^{2+}$ are identifiable in extended structures in the compounds $K_2Re_3S_6 = K_4[Re_6S_8]S_{4/2}(S_2)_{2/2}$[29] and $Ba_2Re_6S_{11} = Ba_2[Re_6$-

(27) Brosset, C. *Ark. Kemi, Mineral. Geol.* **1945**, *A20*, No. 7.
(28) Vaughan, P. A. *Proc. Natl. Acad. Sci. U.S.A.* **1950**, *36*, 461–464.

**Table II.** Parameters Used in EH Calculations

| orbital | $H_{ii}$, eV | $\zeta_1$ [b] | $\zeta_2$ [b] | $C_1$ [a] | $C_2$ [a] |
|---|---|---|---|---|---|
| Mo 4d | −11.06 | 4.54 | 1.90 | 0.5899 | 0.5899 |
| 5s | −8.77 | 1.96 | | | |
| 5p | −5.60 | 1.90 | | | |
| S 3s | −20.0 | 1.817 | | | |
| 3p | −13.3 | 1.817 | | | |
| Se 4s | −20.5 | 2.44 | | | |
| 4p | −14.4 | 2.07 | | | |

[a] Coefficients used in double-$\zeta$ expansion. [b] Slater-type orbital exponents.

**Table III.** Special Point Sets Used for Rhombohedral Brillioun Zone Averages, in Units of $2\pi/a$ [a]

| |
|---|
| Two-Point Set |
| $(1/4, 1/4, 1/4)$ (1), $(1/4, 1/4, -1/4)$ (3) |
| Twelve-Point Set |
| $[(1/8, 1/8, 1/8), (3/8, 3/8, 3/8)]$ (1) each |
| $\left\{\begin{matrix}(1/8, 3/8, 3/8), (3/8, 1/8, -3/8)\\(3/8, 3/8, -1/8), (3/8, -3/8, 1/8)\\(3/8, 1/8, 1/8), (3/8, 1/8, -1/8)\end{matrix}\right\}$ (3) each |

[a] Relative weights are in parentheses.

$S_8]S_3$.[30] In these materials the $Re_6S_8$ clusters are linked together via bridging sulfides and disulfides. Many additional compounds contain clusters with fewer than 24 metal electrons: e.g., $Re_6S_8^{3+}$ is found in $K_2Re_3S_8 = [Re_6S_8]S_{4/2}(S_2)_{2/2}$;[29] $Nb_6I_8^{3+}$ and $Nb_6I_8^{2+}$ are found in $Nb_6I_{11}$[31] and $CsNb_6I_{11}$,[32] respectively.

While the solution-phase chemistry of $Mo_6Cl_8^{4+}$ is well-known, the analogous chemistry of $Mo_6S_8^{4-}$ has not been reported. A first step in this direction has been taken by Michel and McCarley[33] who replaced one of the triply bridging chlorides in $Mo_6Cl_8^{4+}$ by sulfide to obtain a $Mo_6Cl_7S^{3+}$ species. Further developments in this area appear inevitable. Not only do $Mo_6X_8$ species seem promising but the $Mo_9X_{11}$ and $Mo_{12}X_{14}$ systems would be interesting as well. Halide analogues to the larger clusters should also be considered distinct possibilities (Naturally, one can easily imagine that species such as $Nb_9Br_{11}^{2-}$ or $Nb_{12}Br_{14}^{2-}$ would be reasonable as well).

Interestingly, some systems which are isostructural to the those that we have studied do not fit readily into our electron counting schemes. For example, the compounds $Co_6S_8(PEt_3)_6^{+}$ [34] and $Fe_6S_8(PEt_3)_6^{2+}$ [35] clearly have more than 24 electrons per cluster (37 and 30, respectively). Not surprisingly, the metal–metal distances in these molecules are comparatively long (2.79 Å and 2.62 Å), as we would expect on the basis of the occupation of antibonding orbitals for electron counts greater than 24. Similarly, $TlFe_3Te_3$[36] is isostructural to $TlMo_3Se_3$ but clearly is more electron rich (19 electrons per $Fe_3Te_3^-$ unit). In this compound Fe–Fe distances are 2.6 Å, rather long, suggesting that some antibonding bands are filled. Note, however, that Fe–Fe distances may be constrained due to the surrounding large Te atoms.

These and other variations and exceptions notwithstanding, the picture we have presented represents a thread which runs through and ties together our understanding of a beautiful and growing class of compounds. For all their structural and physical diversity, we can see how the similarities in the electronic structure of these compounds are manifested in their structural similarities.

**Acknowledgment.** We thank members of our research group for helpful discussion during the course of this work. Professor M.-H. Whangbo suggested the application of the fragment molecular orbital approach to solids before this work began. Special thanks are due to Sunil Wijeyesekera and Charles Wilker who contributed in the development and programming in adapting to solid-state studies. This work was supported by the National Science Foundation through DMR Grant 7681083 to the Materials Science Center at Cornell and by Grant CHE 7828048.

## Appendix

All calculations were carried out by using the extended Hückel[37] method. Parameters for Mo[38] and S were taken from previous work. Se parameters used in earlier work[23] on these systems were also used in previous calculations.[39] These parameters are found in Table II.

Special points sets used for calculation of overlap populations were obtained by reduction of symmetry from cubic point sets.[17b,c] The two- and twelve-point sets are given in Table III.

**Registry No. 1** (X = S), 57620-25-4; **1** (X = Se), 57620-26-5; **1** (X = Te), 57620-27-6; **6**, 84432-78-0; **7**, 84432-79-1; **9**, 84432-80-4.

(29) Spangenberg, M.; Bronger, W. *Angew. Chem.* **1978**, *90*, 382; *Angew. Chem., Int. Ed. Engl.* **1978**, *17*, 368.
(30) Bronger, W.; Miessen, J.-J. *J. Less-Common Met.* **1982**, 29–38.
(31) (a) Simon, A.; von Schnering, H.-G.; Schäfer, H. *Z. Anorg. Allg. Chem.* **1967**, *355*, 295–310. (b) Imoto, H.; Simon, A. *Inorg. Chem.* **1982**, *21*, 308–319.
(32) Imoto, H.; Corbett, J. D. *Inorg. Chem.* **1980**, *19*, 1241–1245.
(33) Michel, J. B.; McCarley, R. E. *Inorg. Chem.* **1982**, *21*, 1864–1872.
(34) Cecconi, F.; Ghilardi, C. A.; Middolini, S. *Inorg. Chim. Acta* **1982**, *64*, L47–L48.
(35) Cecconi, F.; Ghilardi, C. A.; Middolini, S. *J. Chem. Soc., Chem. Comm.* **1981**, 640–641.
(36) Klepp, K.; Boller, M. *Monatsh. Chem.* **1979**, *110*, 677–684.
(37) Hoffmann, R. *J. Chem. Phys.* **1963**, *39*, 1397–1412.
(38) Kubacek, P.; Hoffmann, R.; Havlas, Z. *Organometallics* **1982**, *1*, 180–188.
(39) Hoffmann, R.; Shaik, S.; Scott, J. C.; Whangbo, M.-H.; Foshee, M. J. *J. Solid State Chem.* **1980**, *34*, 263–269.